

Study of refractive structure in the inelastic $^{16}\text{O}+^{16}\text{O}$ scattering at the incident energies of 250 to 1120 MeV ^{*}

Dao T. Khoa ^{a,b,*}, H.G. Bohlen ^b, W. von Oertzen ^{b,c},
G. Bartnitzky ^d, A. Blazevic ^{b,d}, F. Nuoffer ^d, B. Gebauer ^b,
W. Mittig ^e and P. Roussel-Chomaz ^e

^a*Institute for Nuclear Science and Technique, VAEC, P.O. Box 5T-160,
Nghia Do, Hanoi, Vietnam.*

^b*Hahn-Meitner-Institut GmbH, Glienicker Str. 100, D-14109 Berlin, Germany.*

^c*Fachbereich Physik, Freie Universität Berlin.*

^d*Physikalisches Institut, Universität Tübingen, Auf der Morgenstelle 14, D-72076
Tübingen, Germany.*

^e*GANIL, Bd. Henri Becquerel, BP 5027, F-14021 Caen Cedex, France.*

Abstract

The data of inelastic $^{16}\text{O}+^{16}\text{O}$ scattering to the lowest 2^+ and 3^- excited states of ^{16}O have been measured at $E_{\text{lab}} = 250, 350, 480, 704$ and 1120 MeV and analyzed consistently in the distorted wave Born approximation (DWBA), using the semi-microscopic optical potentials and inelastic form factors given by the folding model, to reveal possible refractive structure of the nuclear rainbow that was identified earlier in the elastic $^{16}\text{O}+^{16}\text{O}$ scattering channel at the same energies. Given the known transition strengths of the 2_1^+ and 3_1^- states of ^{16}O well determined from the (e, e') data, the DWBA description of the inelastic data over the whole angular range was possible only if the absorption in the exit channels is significantly increased (especially, for the $^{16}\text{O}+^{16}\text{O}_{2^+}^*$ exit channel). Although the refractive pattern of the inelastic $^{16}\text{O}+^{16}\text{O}$ scattering was found to be less pronounced compared to that observed in the elastic scattering channel, a clear remnant of the main rainbow maximum could still be seen in the inelastic cross section at $E_{\text{lab}} = 350 - 704$ MeV.

Key words: NUCLEAR REACTIONS

$^{16}\text{O}(^{16}\text{O}, ^{16}\text{O}')^{16}\text{O}^*$, $E_{\text{lab}} = 250, 350, 480, 704$ and 1120 MeV; DWBA and Folding-model analysis, refractive scattering, nuclear rainbow.

PACS: 25.70.Bc, 24.10.Ht, 27.20.+n

1 Introduction

The study of elastic, refractive scattering of light nucleus-nucleus systems, like $^{16}\text{O}+^{16}\text{O}$ and $^{16}\text{O},^{12}\text{C}+^{12}\text{C}$, has proven to be very helpful for our understanding of the interaction between heavy ions (HI) [1]. The main reason is that the refractive structures or *nuclear rainbow* observed in the nucleus-nucleus elastic scattering can provide information on the HI optical potential at small inter-nuclear distances. Although most of the studies have been concentrated on the elastic scattering (see, e.g., Ref. [2] for the $^{16}\text{O}+^{16}\text{O}$ system). The refractive effects have also been found and discussed for one-neutron transfer reactions in the $^{12}\text{C}+^{12}\text{C}$, $^{13}\text{C}+^{12}\text{C}$ [3,4] and $^{16}\text{O}+^{16}\text{O}$ systems [5]. For example, in the $^{16}\text{O}+^{16}\text{O}$ system, where the elastic scattering has shown a pronounced nuclear rainbow pattern [2], a clear remnant of the rainbow pattern was identified in the ϕ_{17015} transfer cross section for the ground state transition to $^{15}\text{O}_{1/2^-}$ [5]. Beside the transfer channel, the inelastic scattering channel of a refractive nucleus-nucleus system can also have a well defined rainbow pattern [6]. In particular, it has been shown recently by Michel and Ohkubo [7] that the transparency seen in some light HI in the form of Airy structure in the elastic scattering channel could have similar pattern in the inelastic scattering channel.

To complete our study [2,5] of the refractive structure in the quasi-elastic $^{16}\text{O}+^{16}\text{O}$ scattering, we present in this work the results of our analysis in the distorted wave Born approximation (DWBA) of the inelastic $^{16}\text{O}(^{16}\text{O},^{16}\text{O}')^{16}\text{O}^*$ scattering data which have been measured in parallel with the elastic $^{16}\text{O}+^{16}\text{O}$ scattering at $E_{\text{lab}} = 250, 350, 480, 704$ and 1120 MeV [8,9,10,11]. These data were taken for the transitions to the lowest 2^+ and 3^- states in ^{16}O at 6.92 MeV and 6.13 MeV excitation energy, respectively, and cover about the same wide angular range as that covered by the elastic scattering and one-neutron transfer data. Since the transition strengths of the 2_1^+ and 3_1^- states of ^{16}O have been accurately determined from the (e, e') data [12,13], they can serve as constraints for the deformation lengths used to generate the inelastic form factors for our DWBA analysis. As a consequence, the measured inelastic scattering data provide a good database for the study of refractive features in the inelastic $^{16}\text{O}(^{16}\text{O},^{16}\text{O}')^{16}\text{O}^*$ scattering.

A brief survey of the measurements of the inelastic $^{16}\text{O}+^{16}\text{O}$ scattering to the 2_1^+ and 3_1^- states of ^{16}O is presented in Sect. 2. The basic ingredients of the

* Research supported, in part, by the Alexander-von-Humboldt Stiftung of Germany, Natural Science Council of Vietnam and Vietnam Atomic Energy Commission (VAEC).

* Corresponding author.

Email addresses: khoa@vaec.gov.vn (Dao T. Khoa), bohlen@hmi.de (H.G. Bohlen), oertzen@hmi.de (W. von Oertzen).

semi-microscopic folding approach to calculate the optical potential and inelastic form factors for the optical model (OM) and DWBA analyses are given in Sect. 3. The DWBA results of the analysis of the inelastic $^{16}\text{O}(^{16}\text{O},^{16}\text{O}')^{16}\text{O}^*$ scattering data at $E_{\text{lab}} = 250 - 1120$ MeV are discussed in Sect. 4. A summary and the main conclusions of this work are given in Sect. 5.

2 Inelastic $^{16}\text{O}(^{16}\text{O},^{16}\text{O}')^{16}\text{O}^*$ data

The experimental spectra have been taken at the incident energies $E_{\text{lab}} = 250 - 480$ MeV [8,9,10] using the Q3D magnetic spectrograph at HMI, and at 704 and 1120 MeV [10,11] using the SPEG spectrograph at GANIL. The spectral lines of the 3^- state at 6.13 MeV and 2^+ state at 6.92 MeV were observed in these spectra as the strongest inelastic transitions. The method used to obtain the experimental cross sections of inelastic scattering from the analysis of the inelastic spectra is described in the following.

Since the projectile and target are identical particles and the same state can be excited in the projectile as well as in the target (and also in both by mutual excitation), every excited state of ^{16}O appears in the spectrum *twice* at the same position of the corresponding excitation energy: (1) a sharp line is observed for the target excitation, and (2) a broad line for the projectile excitation (the mutual excitation could not be inferred from our data due to a small cross section and an increasing three-body background). The line-broadening observed for the excited states of the projectile is due to the recoil momentum of the photon emitted in-flight by the projectile. This effect is directly related to the Doppler-broadening usually observed in the γ -ray spectroscopy. The maximum energy shift in the laboratory system is given by $\Delta E_{\text{max}} = \pm(v/c)E_{\gamma}$ [14], where E_{γ} is the energy of the γ -transition and v is the velocity of the photon-emitting outgoing ^{16}O projectile. These maximum shifts can be rather large: at the forward scattering angles they are, e.g., for the γ -transition from the 2^+ state at 6.92 MeV to the ground state $\Delta E_{\text{max}} = \pm 1.45$ MeV at the beam energy $E_{\text{lab}} = 350$ MeV, and $\Delta E_{\text{max}} = \pm 2.45$ MeV at $E_{\text{lab}} = 1120$ MeV (angular shifts, which also result from the γ -recoil, are small and not larger than the angular resolution). Note that at 1120 MeV, the base width of the broadened line is almost 5 MeV wide, and this needs to be compared with the experimental energy resolution of about 0.5 MeV at both incident energies.

In the spectrum of inelastic excitation the lines resulting from the target excitation are described by Gaussians using the experimental resolution as the width, and the projectile excitation by rectangular distributions with base widths $2(v/c)E_{\gamma}$ which were folded with the experimental resolution. For a given excited state the number of counts for the projectile and target excitation must be equal. This is required by the symmetry of the system which

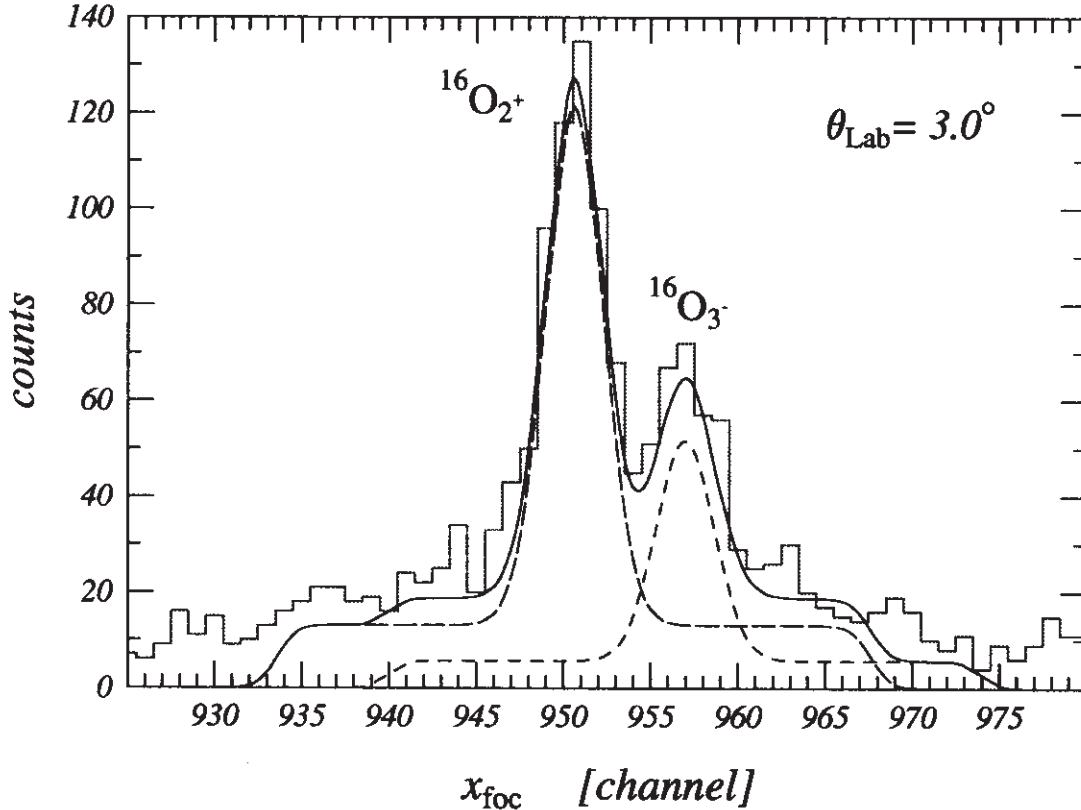


Fig. 1. Spectrum of the inelastic $^{16}\text{O}(^{16}\text{O}, ^{16}\text{O}')^{16}\text{O}^*$ scattering at $E_{\text{lab}} = 1120$ MeV and $\Theta_{\text{lab}} = 3.0^\circ$ in the excitation energy region of the 3^- and 2^+ excited states at 6.13 MeV and 6.92 MeV, respectively. The line shape used for the fit is described in the text.

implies the *equal* excitation strengths of the same excited state in both the projectile and target nuclei at the center-of-mass (c.m.) scattering angles $\Theta_{\text{c.m.}}$ and $\pi - \Theta_{\text{c.m.}}$. Thus, the Gaussian line of the target excitation and the broad line of the projectile excitation have been first normalized to the same area before they were added. The resulting distributions were then fitted to the corresponding excited states in the spectrum by optimizing the normalizations. The fit can be performed simultaneously for several different excited states of ^{16}O with overlapping widths. Fig. 1 shows a spectrum of the inelastic scattering to the 3^- and 2^+ excited states at 6.13 MeV and 6.92 MeV at $E_{\text{lab}} = 1120$ MeV and $\Theta_{\text{lab}} = 3.0^\circ$. The number of counts obtained in the fit of an excited state represents the sum of inelastic cross sections for the projectile and target excitations, which was further divided by a factor of two to obtain the single excitation cross section for the DWBA analysis.

In the analysis of the measured spectra we have used an experimental technique, where two-dimensional plots of scattering angle versus position in the focal plane are constructed to perform projections on either axis by apply-

ing specific gate conditions. To obtain spectra like that shown in Fig. 1 it is necessary to set rather narrow angular gates (typically 0.2° at small angles and slightly larger at intermediate angles) before the spectra are projected to the position axis. This procedure has been applied at the energies of 250, 350, 704, and 1120 MeV up to the scattering angles of 22° , 16.2° , 7.2° , and 9° , respectively, in the laboratory frame. As a result, the angular distributions of the 3^- state at 6.13 MeV and 2^+ state at 6.92 MeV have been well separated in these angular ranges. At larger angles it was not possible to separate the 3^- and 2^+ excited states using this method. Their sum could be, however, easily projected when the gate in excitation energy was set in such a way that both broad lines were included within the acceptable energy limits (in the energy range where other excited states of ^{16}O were not observed). In this way, the angular distribution of the total ($2^+ + 3^-$) cross section has been projected for these states up to 42.5° , 37° , and 19.1° in the laboratory frame at the energies of 250, 350, and 704 MeV, respectively. At 1120 MeV, the range could not be extended due to a steep decrease of the cross sections. At 480 MeV, only the angular distribution of the sum of the ($2^+ + 3^-$) cross sections has been projected.

We also note that the observed spectrum represents overwhelmingly the inelastic scattering to the 3^- and 2^+ excited states at 6.13 MeV and 6.92 MeV, and the strength mixing by the 0^+ and 1^- states at 6.05 MeV and 7.12 MeV can be neglected. While no peak has been observed for the 0^+ state in the angular bin covered by our measurement, a slight rise caused by the 1^- state at 7.12 MeV could be seen. The dipole excitation strength of the 1^- state is however too weak compared to those of the 3^- and 2^+ states: $B(E1 \downarrow) \approx 3.4 \times 10^{-4}$ W.u. compared to $B(E3 \downarrow) \approx 13$ W.u. and $B(E2 \downarrow) \approx 3.5$ W.u. [15], to make a sizable contribution to the total inelastic $^{16}\text{O}(^{16}\text{O}, ^{16}\text{O}')^{16}\text{O}^*$ scattering cross section.

3 Main features of the Folding + DWBA analysis

The most important ingredients of the DWBA analysis of the inelastic scattering $^{16}\text{O}(^{16}\text{O}, ^{16}\text{O}')^{16}\text{O}^*$ are the *complex* optical potentials (OP) in the entrance and exit channels

$$U_{\text{in}}^{(0)} = \langle ^{16}\text{O}, ^{16}\text{O} | V | ^{16}\text{O}, ^{16}\text{O} \rangle, \quad U_{\text{out}}^{(0)} = \langle ^{16}\text{O}^*, ^{16}\text{O} | V | ^{16}\text{O}^*, ^{16}\text{O} \rangle, \quad (1)$$

and the transition potential or inelastic form factor (FF)

$$U_{\text{trans}}^{(\lambda)} = \langle ^{16}\text{O}^*, ^{16}\text{O} | V | ^{16}\text{O}, ^{16}\text{O} \rangle, \quad \text{with } \lambda = 2, 3. \quad (2)$$

For the elastic and inelastic HI scattering, there are two main prescriptions of constructing the nuclear matrix elements (1) and (2):

(I) The phenomenological approach of parameterizing the OP (1) in terms of a conventional Woods-Saxon potential whose parameters to be adjusted to the best fit of elastic scattering data. The inelastic FF (2) is then given by the radial derivative of the OP, scaled by a factor known as the deformation length. This prescription for the inelastic FF is known as the deformed-optical-potential (DOP) model where the deformation length is normally obtained by matching the calculated cross section to the observed inelastic data [16].

(II) The (semi-microscopic) folding approach [17] where the real OP and inelastic FF are calculated microscopically using an appropriate effective in-medium nucleon-nucleon (NN) interaction and the ground-state and transition nuclear densities for the two colliding nuclei.

While the shape of the inelastic folded potential has a strong dependence on the multipolarity λ of the transition, the inelastic FF given by the simple DOP model (I) has a λ -independent shape [18,19]. As a result, the nuclear deformation lengths extracted by the DWBA analysis using the DOP model can be significantly underestimated [18], especially for high multipoles $\lambda \geq 3$.

In the present work, following the success of the folding potential in the OM description of the elastic $^{16}\text{O}+^{16}\text{O}$ scattering [2] and DWBA analysis of the $\phi 17\text{o}15$ one-neutron transfer data at the same energies [5], we use a recent version of the double-folding model [20] to consistently calculate the real OP and inelastic FF for the DWBA analysis of the inelastic $^{16}\text{O}(^{16}\text{O},^{16}\text{O}')^{16}\text{O}^*$ scattering. Within this double-folding approach [20] the projectile-target interaction potential in the elastic or inelastic scattering channel is evaluated as an energy dependent Hartree-Fock-type potential of the dinuclear system

$$V_{\text{F}} = \sum_{i,i' \in A_1; j,j' \in A_2} [\langle i'j' | v_{\text{D}} | ij \rangle + \langle i'j' | v_{\text{EX}} | ji \rangle] = V_{\text{D}} + V_{\text{EX}}, \quad (3)$$

where v_{D} and v_{EX} are the direct and exchange parts of the effective NN interaction. The calculation of $V_{\text{D(EX)}}$ is done iteratively based on a density-matrix expansion method [20,21]. In this calculation, the inputs for mass numbers and incident energies were taken as given by the relativistically corrected kinematics [22]. Like in our earlier works [2,5], we have used for the effective NN interaction $v_{\text{D(EX)}}$ the CDM3Y6 version [23] of the energy- and density dependent M3Y-Paris interaction. Since the density-dependent parameters of the CDM3Y6 interaction were adjusted to reproduce correctly saturation properties of the *infinite* nuclear matter, to use this interaction for a system of two *finite* nuclei one needs to take into account the kinematical transformation from the NN frame to the nucleus-nucleus frame. Thus, the CDM3Y6

interaction was further scaled by a kinematics modification factor deduced from Eq. (19) of Ref. [24]. At the incident energies considered here, this factor leads only to a marginal change of the potential strength (from around 1% at 250 MeV to 5% at 1120 MeV) compared to that given by the same folding approach (3) but neglecting the kinematics modification factor.

To calculate consistently both the optical potential and inelastic form factor one needs to take into account explicitly the multipole decomposition of the nuclear density distribution $\rho(\mathbf{r})$ that enters the folding calculation (see details in Ref. [20])

$$\rho_{JM \rightarrow J'M'}(\mathbf{r}) = \sum_{\lambda\mu} \langle JM\lambda\mu | J'M' \rangle C_\lambda \rho_\lambda(r) [i^\lambda Y_{\lambda\mu}(\hat{\mathbf{r}})]^*, \quad (4)$$

where JM and $J'M'$ are the nuclear spins and their projections in the initial and final states, respectively, $C_0 = \sqrt{4\pi}$ and $C_\lambda=1$ for $\lambda \neq 0$; $\rho_\lambda(r)$ is the nuclear transition density of the 2^λ -pole excitation. In the present work, we adopt the collective-model Bohr-Mottelson prescription [25] to construct the nuclear transition densities for the 2^+ and 3^- excitations of ^{16}O as

$$\rho_\lambda(r) = -\delta_\lambda \frac{d\rho_0(r)}{dr}, \quad \text{with } \lambda = 2, 3. \quad (5)$$

Here $\rho_0(r)$ is the total ground state (g.s.) density and δ_λ is the deformation length of the 2^+ or 3^- excitation of ^{16}O . The g.s. density of ^{16}O was taken as a Fermi distribution with parameters [26] chosen to reproduce the shell-model density for ^{16}O , and the neutron and proton parts of the ^{16}O density were assumed to have the same shape. Such an *isoscalar* assumption for the g.s. density implies [20] that the same nuclear deformation length is used for neutron and proton parts of the transition density (5). These deformation lengths were determined (see Eqs. (3.33)-(3.35) in Ref. [20]) from the measured electric transition strengths of the 2_1^+ and 3_1^- states of ^{16}O , $B(E2 \uparrow) = 40.6 \pm 3.8 \text{ e}^2\text{fm}^4$ [12] and $B(E3 \uparrow) = 1480 \pm 50 \text{ e}^2\text{fm}^6$ [13], so that $\delta_2 = 1.038 \pm 0.048$ and $\delta_3 = 1.825 \pm 0.031 \text{ fm}$ were used to generate the transition densities (5) for the 2_1^+ and 3_1^- states. Given these inputs for the nuclear densities, the (*energy dependent*) real folded optical potential $V_F^{(0)}$ and transition form factors $V_F^{(2)}$ and $V_F^{(3)}$ were obtained straightforwardly in the double-folding approach [20]. Along with the nuclear FF, the Coulomb inelastic form factor $V_C^{(\lambda)}$ was calculated by the same folding method (3), using the g.s. and transition *charge* densities of the two colliding ^{16}O nuclei and the Coulomb interaction between the two protons.

To have the *complex* energy dependent optical potentials for the entrance and exit channels, the real (folded) OP was further added, as in our previous folding analyses, by a Woods-Saxon (WS) imaginary potential that contains

both the volume and surface terms. Thus, the OP used in the present DWBA analysis is

$$U_{\text{in(out)}}^{(0)}(R) = V_{\text{C}}^{(0)}(R) + N_{\text{V}}^{(0)}V_{\text{F}}^{(0)}(R) - i[W_{\text{V}}(R) + W_{\text{D}}(R)]. \quad (6)$$

Here $V_{\text{C}}^{(0)}$ is the elastic Coulomb potential between a point charge and a uniform charge distribution of radius $R_{\text{C}} = 1.3 \times (A_1^{1/3} + A_2^{1/3})$ fm and the volume and surface parts of the imaginary WS potential are determined as

$$W_{\text{V}}(R) = W_{\text{V}}\{1 + \exp[(r - R_{\text{V}})/a_{\text{V}}]\}^{-1}, \quad (7)$$

$$W_{\text{D}}(R) = 4W_{\text{D}} \exp[(R - R_{\text{D}})/a_{\text{D}}]\{1 + \exp[(R - R_{\text{D}})/a_{\text{D}}]\}^{-2}. \quad (8)$$

For $U_{\text{in}}^{(0)}$, the renormalization factor $N_{\text{V}}^{(0)}$ of the real folded potential $V_{\text{F}}^{(0)}$ and parameters of the WS imaginary potential were adjusted in each case to the best fit of the measured elastic $^{16}\text{O}+^{16}\text{O}$ scattering data [2]. It is commonly assumed in the DWBA analysis of inelastic nucleus-nucleus scattering [16], especially when one uses the DOP model for the inelastic FF, that $U_{\text{out}}^{(0)} = U_{\text{in}}^{(0)}$. In the present work, given the highly accurate inelastic $^{16}\text{O}(^{16}\text{O}, ^{16}\text{O}')^{16}\text{O}^*$ scattering data and inelastic folded FF's fixed by the known transition strengths of the 2_1^+ and 3_1^- states of ^{16}O , we find that this assumption is not always a good approximation, and it could lead to an underestimation of the transition strength of the nuclear excitation when the refractive effect is strong.

Within the folding model [20], the following *complex* energy dependent inelastic FF is often used for the transition potential (2)

$$U_{\text{trans}}^{(\lambda)}(R) = V_{\text{C}}^{(\lambda)}(R) + N_{\text{V}}^{(\lambda)}V_{\text{F}}^{(\lambda)}(R) - i\delta_{\lambda} \frac{dW_{\text{in}}(R)}{dR}, \quad \text{where } \lambda = 2, 3, \quad (9)$$

and $W_{\text{in}}(R) = W_{\text{V}}(R) + W_{\text{D}}(R)$ is the WS imaginary part of $U_{\text{in}}^{(0)}(R)$. With the deformation length fixed by the known transition strength, the renormalization factor $N_{\text{V}}^{(\lambda)}$ of the real folded FF is usually adjusted to the best DWBA fit of inelastic scattering data and it should be close to unity for the folding procedure (9) to be meaningful. All the OM and DWBA calculations were made using the code ECIS97 written by Raynal [27].

4 Results of the DWBA analysis and discussion

To have a reliable DWBA description of the inelastic $^{16}\text{O}(^{16}\text{O}, ^{16}\text{O}')^{16}\text{O}^*$ scattering, one needs first to determine the parameters of the OP (1) for the

Table 1

OP parameters (6)-(8) for the entrance and exit channels used in the DWBA analysis of the inelastic $^{16}\text{O}(^{16}\text{O}, ^{16}\text{O}')^{16}\text{O}^*$ scattering at incident energies of 250 to 1120 MeV. J_V and J_W are the volume integrals (per interacting nucleon pair) of the real folded potential and of the imaginary WS potential, respectively. If blank, the values are the same as those in the preceding row.

E_{lab} (MeV)	channel	$N_V^{(0)}$	J_V (MeVfm ³)	W_V (MeV)	R_V (fm)	a_V (fm)	W_D (MeV)	R_D (fm)	a_D (fm)	J_W (MeVfm ³)
250	entrance	0.781	290.0	38.34	4.405	0.949	6.630	5.657	0.483	98.81
	exit (2 ⁺)			48.46						119.4
	exit (3 ⁻)			34.87						91.76
350	entrance	0.845	298.2	25.32	5.832	0.629	6.932	4.846	0.350	103.0
	exit (2 ⁺)			35.76						140.8
	exit (3 ⁻)			27.00						109.1
480	entrance	0.791	261.5	31.59	5.421	0.711	1.647	5.114	0.415	99.88
	exit (2 ⁺)			41.89			15.75			161.9
	exit (3 ⁻)			33.89			6.586			117.6
704	entrance	0.867	256.1	28.62	5.669	0.652	7.095	4.153	0.450	107.7
	exit (2 ⁺)			39.96			6.010			144.2
	exit (3 ⁻)			32.14			6.862			119.1
1120	entrance	0.905	218.6	46.34	4.793	0.809	0.868	5.640	0.391	109.1
	exit (2 ⁺)			61.98			3.888			152.7
	exit (3 ⁻)			50.30			1.178			119.0

entrance and exit channels. In addition to the scaling the CDM3Y6 interaction by a kinematics modification factor, a more accurate local approximation [21] was also used for the exchange potential V_{EX} compared to the folded potentials used earlier in Ref. [2]. Therefore, we have made again a detailed OM analysis of the elastic $^{16}\text{O}+^{16}\text{O}$ scattering data [8,9,10,11] using the complex OP (6). The obtained OP parameter sets (see the best-fit OP parameters for the $^{16}\text{O}+^{16}\text{O}$ entrance channel at different incident energies in Table 1) reproduce the same refractive structure in the elastic $^{16}\text{O}+^{16}\text{O}$ cross sections as that reported in Ref. [2]. Note that the improved folding procedure leads to a slightly smaller renormalization factor $N_V^{(0)}$ of the real folded potential at all energies, with the largest difference of about 10% found at 250 MeV. The corresponding volume integrals J_V are changed only by about 2-5% and they indicate practically the same potential family for the real OP as that discussed in Ref. [2].

To show more clearly the evolution of the refractive Airy pattern with the increasing incident energy, we have plotted in Fig. 2 the measured elastic $^{16}\text{O}+^{16}\text{O}$ data and the calculated cross sections versus the momentum transfer $q = 2k \sin(\Theta_{\text{c.m.}}/2)$, where k is the wave number of the projectile. In such a presentation, the location of the first Airy minima (A1) can be traced up to the energy of 704 MeV. The rainbow pattern associated with A1 [2] is somewhat obscured at $E_{\text{lab}} = 250$ MeV by the Mott interference caused by boson symmetry between the two identical ^{16}O nuclei, but it becomes more prominent at $E_{\text{lab}} = 350$ MeV. Actually, the elastic data at 350 MeV [9] is now known as a very clear experimental evidence of the nuclear rainbow scattering pattern in elastic heavy-ion scattering. In the present work we investigate whether this rainbow pattern also exists in the inelastic $^{16}\text{O}(^{16}\text{O},^{16}\text{O}')^{16}\text{O}^*$ scattering channels.

As discussed earlier in Ref. [2], a very consistent absolute angular calibration was obtained for the elastic $^{16}\text{O}+^{16}\text{O}$ scattering data at $E_{\text{lab}} = 1120$ MeV, where all the gauging conditions were well fulfilled for the target constituents ^6Li , ^{12}C , ^{16}O , ^{40}Ca and ^{51}V simultaneously. The inelastic $^{16}\text{O}(^{16}\text{O},^{16}\text{O}')^{16}\text{O}^*$ scattering data were also quite accurately measured at this energy, with the inelastic scattering cross sections for the 2^+ and 3^- states of ^{16}O well separated over the whole angular range covered by the elastic scattering data. Since the DWBA formalism also works better at medium and high energies (where the coupled-channel effects are not significant [16]), we started first our DWBA analysis of the inelastic scattering data at 1120 MeV, and the DWBA results are compared with the measured $^{16}\text{O}(^{16}\text{O},^{16}\text{O}')^{16}\text{O}^*$ angular distributions in Fig. 3. Given the deformation lengths fixed above by the measured electric transition rates of the 2^+ and 3^- states and the validity of DWBA, the *complex* FF's (9) of the inelastic scattering to these states were expected to give some reasonable description of the data with the unrenormalized folded FF ($N_V^{(2)} = N_V^{(3)} = 1$). However, the DWBA calculation based on such an assumption, using the same complex OP in the entrance and exit channels, turned out to grossly overestimate the measured angular distributions for the 2^+ and 3^- states of ^{16}O (see dotted curves in Fig. 3). Even if we assume lower values for the deformation lengths, $\delta_{2(3)} \Rightarrow \delta_{2(3)} - \Delta\delta_{2(3)}$ where $\Delta\delta_{2(3)}$ are the experimental uncertainties of the adopted $\delta_{2(3)}$ values discussed in Sec. 3, the absolute 2^+ and 3^- cross sections are reduced only by around 10% and 4%, respectively. Such a small change in the inelastic cross section is almost invisible in the logarithmic scale of the plot.

We tried further to adjust the renormalization factors of the real folded FF's to best fit the data, using the same imaginary inelastic FF's. These factors then turned out to be significantly smaller than unity: $N_V^{(2)} \approx 0.54$ and $N_V^{(3)} \approx 0.06$ which are too unrealistic. Moreover, with $N_V^{(3)}$ approaching almost zero, the strength of the imaginary 3^- inelastic FF is still so strong that the DWBA cross section is roughly twice the measured cross section over the whole angular

range. Keeping $N_V^{(3)}$ value within the range of 0.7-1.0, which is close to $N_V^{(0)}$ values obtained in numerous folding analyses of elastic α -nucleus and nucleus-nucleus scattering, a reasonable description of the data could only be reached by switching off the imaginary part of $U_{\text{trans}}^{(3)}$ (see dashed and dash-dotted curves in the lowest part of Fig. 3 which were obtained with $N_V^{(3)} = 0.938$ and 1, respectively). For the 2^+ excitation, even after the imaginary part of $U_{\text{trans}}^{(2)}$ is neglected, we could not get a good description of the measured cross section for the 2^+ state over the whole angular range. If the real folded FF is renormalized by $N_V^{(2)} \approx 0.63$ (a strong *quenching* of the transition strength), the DWBA result fits reasonably the data at large angles but underestimates significantly the 2^+ data at forward angles (dashed curve in the middle part of Fig. 3). When the real folded FF is kept unchanged ($N_V^{(2,3)} = 1$), the DWBA calculation can only fit the data points at smallest angles and strongly overestimate the data at large angles (dash-dotted curve in the middle part of Fig. 3). An overall good description of the measured 2^+ cross section could finally be reached only when a more absorptive OP is used for the $^{16}\text{O}+^{16}\text{O}_{2^+}$ exit channel, with the absorption strength around 40 to 60% stronger than that in the entrance channel (see Table 1). In this case, we have used the real folded FF with $N_V^{(2,3)} = 1$ and the same WS geometry of the $^{16}\text{O}+^{16}\text{O}^*$ imaginary OP as that in the $^{16}\text{O}+^{16}\text{O}$ entrance channel, only the WS strengths of the imaginary OP in the exit channel were adjusted to obtain a good description of the inelastic scattering data by the DWBA calculation. For the 3^- excitation, such a procedure lead only to a slightly more absorptive OP in the $^{16}\text{O}+^{16}\text{O}_{3^-}$ exit. The situation remains nearly the same when we switch on the 3-channel coupling $2^+ \leftrightarrow 0^+ \leftrightarrow 3^-$. The coupled-channel (CC) calculation using the same OP and inelastic FF as those used in the DWBA calculation leads to a slight reduction (around 10-30%) of the inelastic cross sections at largest angles (compare solid and dash-dotted curves in Fig. 4). After the depths of the WS imaginary potentials were re-adjusted to fit the data in the CC calculation (the dotted curves in Fig. 4), the absorptive strength of the OP is reduced by only around 5-6%. Such a weak CC effect shown in Fig. 4 confirms the conclusion made based on the DWBA results plotted in Fig. 3.

We have further analyzed the $^{16}\text{O}(^{16}\text{O},^{16}\text{O}')^{16}\text{O}^*$ data at the lower energies. Since the excitation energies of the 2^+ and 3^- states of ^{16}O are separated by about 0.8 MeV, the inelastic cross sections for these two states could not be well separated at large angles due to stronger kinematical effects. There only the sum of the 2^+ and 3^- cross sections could be measured. We had to maintain, therefore, in each case a good DWBA description of both the 2^+ and 3^- data at forward angles as well as their sum at large angles, in the refractive angular region. Our DWBA analysis of the considered inelastic $^{16}\text{O}(^{16}\text{O},^{16}\text{O}')^{16}\text{O}^*$ data at lower energies shows consistently that the inelastic scattering to the lowest 2^+ and 3^- states of ^{16}O exhausts mainly the strength of the *real* part of the inelastic FF (9).

If we consider the imaginary part of the inelastic FF as originating from a ‘dynamic polarization’ of the transition potential, similar to that of the microscopic OP according to Feshbach [28], then these results would indicate a dominance of the direct (one-step) inelastic scattering process and the contribution from higher order terms to the $^{16}\text{O}(^{16}\text{O}, ^{16}\text{O}')^{16}\text{O}^*$ reaction is negligible. A similar conclusion has also been made recently by Katsuma *et al.* [29] based on their detailed CC analysis of the elastic and inelastic $^{16}\text{O}+^{16}\text{O}$ scattering at 350 MeV.

The DWBA results obtained with the inelastic FF consisting only of the real folded FF are shown in Fig. 5. Since a renormalization of the real folded FF usually could not deliver a good DWBA description of the data over the whole angular range and given the dominance of the direct one-step scattering process, we have used throughout our DWBA analysis $N_V^{(\lambda)} = 1$ and δ_λ values given in Sec. 3. These DWBA results confirm again that a significantly more absorptive OP must be used for the exit channels, especially for $^{16}\text{O}+^{16}\text{O}_{2+}$ where the absorption was found roughly 40-50% stronger than that in the $^{16}\text{O}+^{16}\text{O}$ entrance channel (see the volume integral J_W of the absorptive WS potential in Table 1). We note that the enhancement of the absorption found for the $^{16}\text{O}+^{16}\text{O}^*$ exit channels is very similar to the enhanced absorption established earlier in our (finite-range) DWBA analysis of the one-neutron transfer $\phi 17\text{o}15$ reaction [5], where the absorption in the $^{17}\text{O}+^{15}\text{O}$ exit channels is also about 50% or more stronger than that in the $^{16}\text{O}+^{16}\text{O}$ entrance, with the corresponding volume integrals J_W of the absorptive WS potential close to those normally observed for a HI system with strong absorption. Since the enhanced absorption implies a shorter mean free path [30,31], our DWBA results for the inelastic $^{16}\text{O}(^{16}\text{O}, ^{16}\text{O}')^{16}\text{O}^*$ scattering also support the conclusion of Ref. [5] that the nuclear mean free path is quite different as one considers different reaction channels. The nuclear mean free path in the overlapping region was shown [5] to gradually decrease when one goes from a tightly bound and spherical double closed-shell nucleus ^{16}O to a less bound ^{15}O nucleus (in its ground and excited $p_{3/2}$ states). Now we see the same trend for the ^{16}O nucleus in the excited 2^+ and 3^- states. Thus, the enhanced absorption found in the exit channels should, in general, imply a shorter mean free path of the excited (and less-bound) nuclear cluster in the nuclear medium. To illustrate the trend of the increased absorption in the exit channels of the quasi-elastic $^{16}\text{O}+^{16}\text{O}$ scattering, we have plotted in Fig. 6 the volume integral of the absorptive WS potential J_W per interacting nucleon pair. While a volume integral $J_W \approx 100 \text{ MeV fm}^3$ was found for the elastic $^{16}\text{O}+^{16}\text{O}$ scattering channel, with the weakening or even disappearance of refractive effects in the inelastic $^{16}\text{O}(^{16}\text{O}, ^{16}\text{O}')^{16}\text{O}^*$ scattering and one-neutron $\phi 17\text{o}15$ transfer channels [5] the correct description of the data over a large angular range required consistently an increased absorption in the exit channels. For the inelastic scattering to the excited 2^+ state of ^{16}O and one-neutron transfer to the excited $3/2^-$ state of ^{15}O , the enhanced absorption has lead to a volume

integral J_W up to around 150-200 MeV fm³ (see Fig. 6) which is close to that observed for strong-absorbing HI systems. For example, the OM analysis of the elastic scattering of 390 MeV ²⁰Ne on ¹²C using the real WS and folded potentials has given $J_W = 207$ MeV fm³ and 155 MeV fm³, respectively [8].

The enhanced absorption found for the exit channels of the inelastic ¹⁶O+¹⁶O scattering and $\phi 17\text{o}15$ transfer reaction stresses the need to have a realistic choice for the OP not only in the entrance but also in the exit channel. The use of the same complex OP in both the entrance and exit channels might lead to a large uncertainty in the deduced transition strength if one follows the standard method of scaling the inelastic FF to match the DWBA results to the measured angular distributions. In particular, one needs to be aware of this effect while analyzing the inelastic scattering data measured at ‘refractive’ energies for a light HI system containing an unstable nucleus with the excited state being either unbound or very weakly bound. We note finally that the subtle effect of absorption enhancement could have been found only owing to very accurately measured inelastic ¹⁶O(¹⁶O, ¹⁶O’)¹⁶O* scattering and one-neutron $\phi 17\text{o}15$ transfer data which cover a wide angular range and about 6 orders of the cross-section magnitude.

We consider now the refractive features in the inelastic ¹⁶O(¹⁶O, ¹⁶O’)¹⁶O* scattering in more details, and the best data set for this purpose are those measured at $E_{\text{lab}} = 350$ MeV. At this energy, a broad shoulder-like primary rainbow pattern preceded by the first Airy minimum at $\Theta_{\text{c.m.}} \approx 44^\circ$ (or $q \approx 6.1$ fm⁻¹) has been observed in the elastic ¹⁶O+¹⁶O scattering cross section (see Fig. 2). From the DWBA results given by the same OP in the entrance and exit channel (dotted and dash-dotted curves) for the inelastic scattering at 350 MeV shown in Fig. 7 one can see a weak rise in the sum of the 2⁺ and 3⁻ cross sections at $\Theta_{\text{c.m.}} \geq 46^\circ$. This broad pattern at large angles is about the same for the 2⁺ and 3⁻ cross sections (with overlaid oscillatory structures at the forward angles which are out of phase) and should be of the refractive nature and caused by the same interference mechanism that gives rise to the Airy oscillation seen in the elastic ¹⁶O+¹⁶O scattering [7]. Note that the rainbow shoulder is slightly shifted towards large angles because of a small decrease of the c.m. energy in the exit channel. This structure becomes weaker if one uses a more absorptive OP in the exit channels to reproduce the measured (2⁺ + 3⁻) cross section as discussed above. Nevertheless, a remnant of the primary rainbow shoulder can still be seen separately in the calculated 2⁺ and 3⁻ cross sections as well as in the measured total cross section. From the calculated and measured ¹⁶O(¹⁶O, ¹⁶O’)¹⁶O* cross sections at all energies shown in Fig. 5 one can trace this weak rainbow pattern in the inelastic scattering cross section from the energy of 350 MeV up to 704 MeV.

At 250 MeV, the nuclear rainbow pattern of the elastic ¹⁶O+¹⁶O scattering was shown to be shifted to scattering angles larger than 90° [2] and there it

is invisible due to the strong Mott interference. That is also the reason why one can not see it in the inelastic $^{16}\text{O}(^{16}\text{O},^{16}\text{O}')^{16}\text{O}^*$ scattering. Interestingly, the enhancement of absorption found at higher energies is not very obvious at 250 MeV where the results given by the same OP for both the entrance and exit channels deliver also a fairly good description of the measured data (see Fig. 8). We have seen the same trend in our recent DWBA analysis of the one-neutron $\text{O}^{17}\text{O}^{15}$ reaction [5], where the enhanced absorption in the exit channel was also not observed at 250 MeV. It is very likely that the enhancement of the absorption in the exit channel is a feature associated with the refractive nature of quasi-elastic nucleus-nucleus scattering. Such an effect can be well expected from the interpretation of the rainbow scattering as a phenomenon associated with a *weak absorption* which allows a *deeper interpenetration* of the two nuclei, with the refractive pattern determined by the nucleus-nucleus potential at small distances [32].

Given a weak rainbow pattern seen in the inelastic scattering cross section at the energies of 350-704 MeV, one might also expect some sensibility of the measured inelastic data to the shape of the nucleus-nucleus form factor at small distances. To probe this effect, we have constructed the transition form factors (2) using both the folding and DOP methods. To obtain the DOP form factors, we have first deformed the (best-fit) elastic folded potential by the same deformation lengths δ_λ as that used to generate the nuclear transition densities (5) for the folding calculation. Although the two choices of the FF have more or less the same strength at the surface of the dinuclear system, they differ from each other substantially at small radii (compare the solid and dotted curves in Fig. 9). This difference shows up clearly in the calculated inelastic cross section and one can see from Fig. 10 that a reasonable DWBA description of the data by the DOP form factors can only be reached when the deformation lengths $\delta_{2,3}$ used in the DOP model are substantially reduced, especially, for the $\lambda = 3$ case where δ_3 has to be reduced by a factor around 1.67. The corresponding transition rate is then reduced to $B(E3 \uparrow) \approx 531 e^2\text{fm}^6$ which is nearly three times smaller than the adopted experimental value of $1480 \pm 50 e^2\text{fm}^6$ [13]. Such a deficiency of the DOP form factor, which leads to an artificial “hindrance” of the 3^- excitation strength, has been first pointed out by Beene et al. [18] and is now confirmed again by our folding + DWBA analysis of the inelastic $^{16}\text{O}(^{16}\text{O},^{16}\text{O}')^{16}\text{O}^*$ scattering. Moreover, with the inelastic scattering data covering a wide angular range, it can be seen in Fig. 10 that the DOP method completely fails to give a good description of the data points at largest angles which are known to be sensitive to the shape of the FF at small distances. Like the rainbow pattern in the elastic $^{16}\text{O}+^{16}\text{O}$ scattering which can be used to probe the real OP at small internuclear distances [32], we have established that the weak remnant of the primary rainbow observed in the inelastic $^{16}\text{O}(^{16}\text{O},^{16}\text{O}')^{16}\text{O}^*$ scattering at 350 MeV is also helpful in testing the inelastic FF at small radii.

5 Summary

Inelastic $^{16}\text{O}(^{16}\text{O},^{16}\text{O}')^{16}\text{O}^*$ scattering data at $E_{\text{lab}} = 250, 350, 480, 704$ and 1120 MeV for the transitions to the lowest 2^+ and 3^- states in ^{16}O , covering the same wide angular range as that covered by the elastic $^{16}\text{O}+^{16}\text{O}$ scattering at these energies [8,9,10,11], have been measured and analyzed within the DWBA using the semi-microscopic optical potential and inelastic form factor given by the folding model [20]. Although the refractive pattern of the inelastic $^{16}\text{O}(^{16}\text{O},^{16}\text{O}')^{16}\text{O}^*$ scattering was found less pronounced compared to that observed in the elastic scattering channel, a similar evolution of the primary rainbow remnant could still be traced in the inelastic scattering cross section up to $E_{\text{lab}} = 704$ MeV.

Given the strengths of the folded form factors fixed by the deformation lengths determined from the experimental $B(E2 \uparrow)$ and $B(E3 \uparrow)$ data [12,13], a reasonable DWBA description of the measured 2^+ and 3^- angular distributions has been obtained only if the absorption in exit channels is significantly increased, especially for the $^{16}\text{O}+^{16}\text{O}_{2+}$ exit, at the energies where the refractive (rainbow) pattern was well observed in the elastic scattering channel. Our DWBA analysis also shows consistently that the considered inelastic scattering to the lowest 2^+ and 3^- states of ^{16}O exhausts mainly the strength of the *real* part of the inelastic form factor (9). In terms of Feshbach's formalism [28], these results should indicate the dominance of the direct (one-step) inelastic scattering and negligible contribution from higher order terms to the $^{16}\text{O}(^{16}\text{O},^{16}\text{O}')^{16}\text{O}^*$ reaction.

The enhanced absorption found for the exit channels of the inelastic $^{16}\text{O}+^{16}\text{O}$ scattering and $\text{o}17\text{o}15$ transfer reaction [5] indicates that the nuclear mean free path is decreasing during the transition from the entrance channel containing two tightly bound double closed-shell ^{16}O nuclei in their ground states to a *less bound* exit channel containing either ^{15}O nucleus or ^{16}O nucleus in the excited 2^+ or 3^- states. This would be of interest to study this effect in the future analysis of the quasi-elastic scattering data measured for the nucleus-nucleus systems involving unstable nuclei, where the partitions in the entrance and exit channels are very differently bound.

The weak rainbow remnant observed in the inelastic $^{16}\text{O}(^{16}\text{O},^{16}\text{O}')^{16}\text{O}^*$ scattering was shown to be quite helpful in testing the inelastic FF at small radii. A comparison made between the folding and DOP models for the inelastic form factor shows clearly the failure of the DOP approach in the description of the inelastic $^{16}\text{O}(^{16}\text{O},^{16}\text{O}')^{16}\text{O}^*$ scattering data at 350 MeV, which cover both the diffractive and refractive regions in the angular distribution. The use of the DOP model also significantly underestimates the deformation lengths of the nuclear excitations, especially for $\lambda \geq 3$. Therefore, we recommend

again the folding model as a more reliable tool in the analysis of the inelastic nucleus-nucleus scattering.

Acknowledgements

One of the authors (D.T.K.) thanks the Hahn-Meitner-Institut Berlin and the Alexander-von-Humboldt Stiftung of Germany for the financial support and hospitality during his stays at HMI Berlin in 2000, 2001 and 2003 to work on this project. The comment by Ken Amos on the kinematical transformation of the NN interaction from the NN frame to the nucleus-nucleus frame is also appreciated.

References

- [1] M.E. Brandan, G.R. Satchler, *Phys. Rep.* 285 (1997) 143.
- [2] Dao T. Khoa, W. von Oertzen, H.G. Bohlen, F. Nuoffer, *Nucl. Phys. A* 672 (2000) 387.
- [3] H.G. Bohlen, X.S. Chen, J.G. Cramer, P. Fröbrich, B. Gebauer, H. Lettau, A. Miczaika, W. von Oertzen, R. Ulrich, Th. Wilpert, *Z. Phys. A* 322 (1985) 241.
- [4] G.R. Satchler, *Nucl. Phys. A* 505 (1989) 103.
- [5] H.G. Bohlen, Dao T. Khoa, W. von Oertzen, B. Gebauer, F. Nuoffer, G. Bartnitzky, A. Blazevic, W. Mittig, P. Roussel-Chomaz, *Nucl. Phys. A* 703 (2002) 573.
- [6] Dao T. Khoa, O.M. Knyazkov, *Z. Phys. A* 328 (1987) 67.
- [7] F. Michel, S. Ohkubo, *Phys. Rev. C* 70 (2004) 044609.
- [8] H.G. Bohlen, E. Stiliaris, B. Gebauer, W. von Oertzen, M. Wilpert, Th. Wilpert, A. Ostrowski, Dao T. Khoa, A.S. Demyanova, A.A. Ogloblin, *Z. Phys. A* 346 (1993) 189.
- [9] E. Stiliaris, H.G. Bohlen, P. Fröbrich, B. Gebauer, D. Kolbert, W. von Oertzen, M. Wilpert, Th. Wilpert, *Phys. Lett. B* 223 (1989) 291.
- [10] G. Bartnitzky, A. Blazevic, H.G. Bohlen, J.M. Casandjian, M. Chartier, H. Clement, B. Gebauer, A. Gillibert, Th. Kirchner, Dao T. Khoa, A. Lepine-Szily, W. Mittig, W. von Oertzen, A.N. Ostrowski, P. Roussel-Chomaz, J. Siegler, M. Wilpert, Th. Wilpert, *Phys. Lett. B* 365 (1996) 23.
- [11] F. Nuoffer, G. Bartnitzky, H. Clement, A. Blazevic, H.G. Bohlen, B. Gebauer, W. von Oertzen, M. Wilpert, Th. Wilpert, A. Lepine-Szily, W. Mittig, A.N. Ostrowski, P. Roussel-Chomaz, *Il Nuovo Cimento* 111 A (1998) 971.

- [12] S. Raman, C.W. Nestor Jr., P. Tikkanen, *At. Data and Nucl. Data Tables* 78 (2001) 1.
- [13] T. Kibedi, R.H. Spear, *At. Data and Nucl. Data Tables* 80 (2002) 35.
- [14] H.G. Bohlen, W. Bohne, B. Gebauer, W. von Oertzen, M. Goldschmidt, H. Hafner, L. Pflug, K. Wannebo, *Phys. Rev. Lett.* 37 (1976) 195.
- [15] P.M. Endt, *At. Data and Nucl. Data Tables* 23 (1979) 3; *ibid.* 55 (1993) 171.
- [16] G.R. Satchler, *Direct Nuclear Reactions*, Clarendon Press, Oxford, 1983.
- [17] G.R. Satchler, W.G. Love, *Phys. Rep.* 55 (1979) 183.
- [18] J.R. Beene, D.J. Horen, G.R. Satchler, *Phys. Lett. B* 344 (1995) 67.
- [19] J.R. Beene, D.J. Horen, G.R. Satchler, *Nucl. Phys. A* 596 (1996) 137.
- [20] Dao T. Khoa, G.R. Satchler, *Nucl. Phys. A* 668 (2000) 3.
- [21] Dao T. Khoa, *Phys. Rev. C* 63 (2001) 034007.
- [22] M.E. Farid, G.R. Satchler, *Phys. Lett. B* 146 (1984) 389.
- [23] Dao T. Khoa, G.R. Satchler, W. von Oertzen, *Phys. Rev. C* 56 (1997) 954.
- [24] W.G. Love, M.A. Franey, *Phys. Rev. C* 24 (1981) 1073.
- [25] A. Bohr, B.R. Mottelson, *Nuclear Structure*, Benjamin, New York, 1975, Vol.2.
- [26] M.E. Farid, G.R. Satchler, *Nucl. Phys. A* 438 (1985) 525.
- [27] J. Raynal, *Computing as a Language of Physics*, IAEA, Vienna, 1972, p.75; J. Raynal, coupled-channel code ECIS97 (unpublished).
- [28] H. Feshbach, *Theoretical Nuclear Physics*, Vol. II, Wiley, New York, 1992.
- [29] M. Katsuma, Y. Sakuragi, S. Okabe, Y. Kondo, *Prog. Theor. Phys.* 107 (2002) 377.
- [30] J.P. Jeukenne, A. Lejeune, C. Mahaux, *Phys. Rep.* 25 (1976) 83; *Phys. Rev. C* 16 (1977) 80.
- [31] J.W. Negele, K. Yazaki, *Phys. Rev. Lett.* 47 (1981) 71.
- [32] W. von Oertzen, H.G. Bohlen, Dao T. Khoa, *Nucl. Phys. A* 722 (2003) 202c.

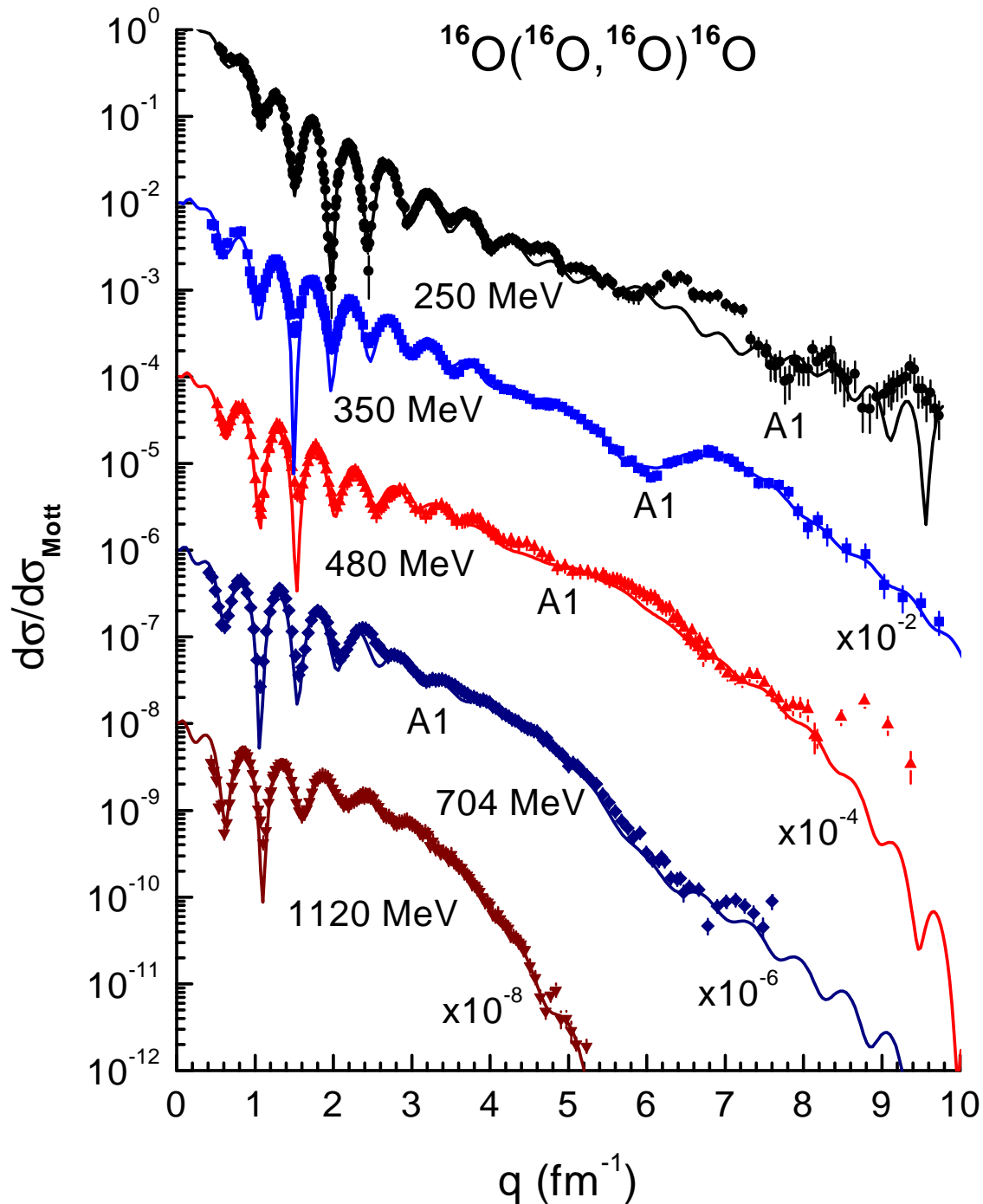


Fig. 2. The OM description of the elastic $^{16}\text{O}+^{16}\text{O}$ scattering data measured at $E_{\text{lab}} = 250 - 1120$ MeV [8,9,10,11] given by the semi-microscopic optical potential (6). The OP parameters are those determined for the entrance $^{16}\text{O}+^{16}\text{O}$ channel (see Table 1). The cross sections are given in ratio to the Mott cross section and plotted versus the momentum transfer $q = 2k \sin(\Theta_{\text{c.m.}}/2)$, where k is the wave number of the projectile. A1 indicates location of the first Airy minimum.

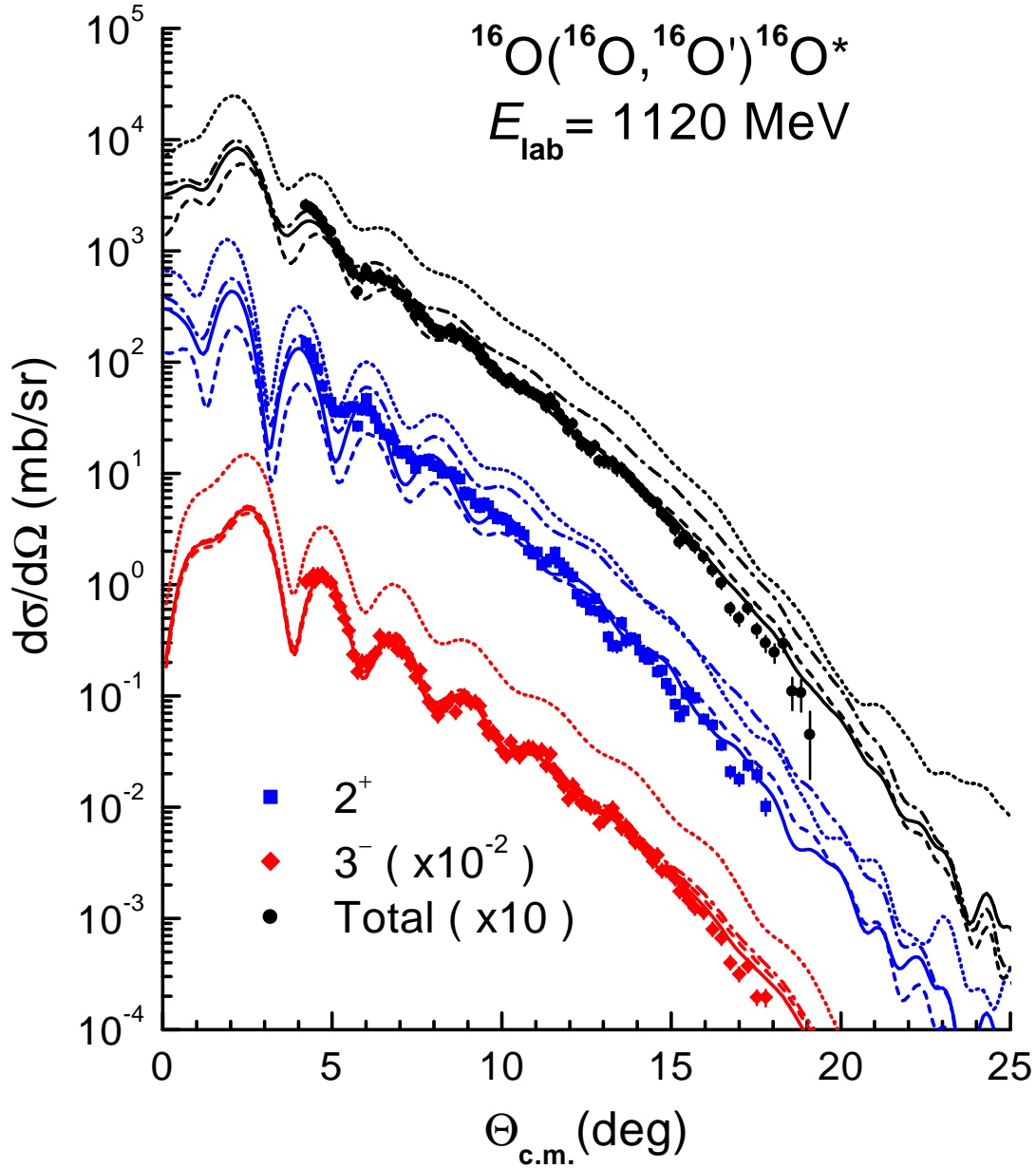


Fig. 3. The calculated DWBA cross sections for the inelastic $^{16}\text{O}(^{16}\text{O}, ^{16}\text{O}')^{16}\text{O}^*$ scattering at $E_{\text{lab}} = 1120 \text{ MeV}$ in comparison with the measured 2^+ and 3^- inelastic cross sections and their sum. The dotted curves are results given by the original ($N_V^{(2,3)} = 1$) *complex* inelastic FF [see Eq. (9)], dash-dotted curves are given by the original *real* folded FF only, dashed curves are given by the real folded FF which were renormalized to the best fit the data, and solid curves are obtained with the original real folded FF but using a *more absorptive* OP in the $^{16}\text{O}+^{16}\text{O}^*$ exit channels (see Table 1).

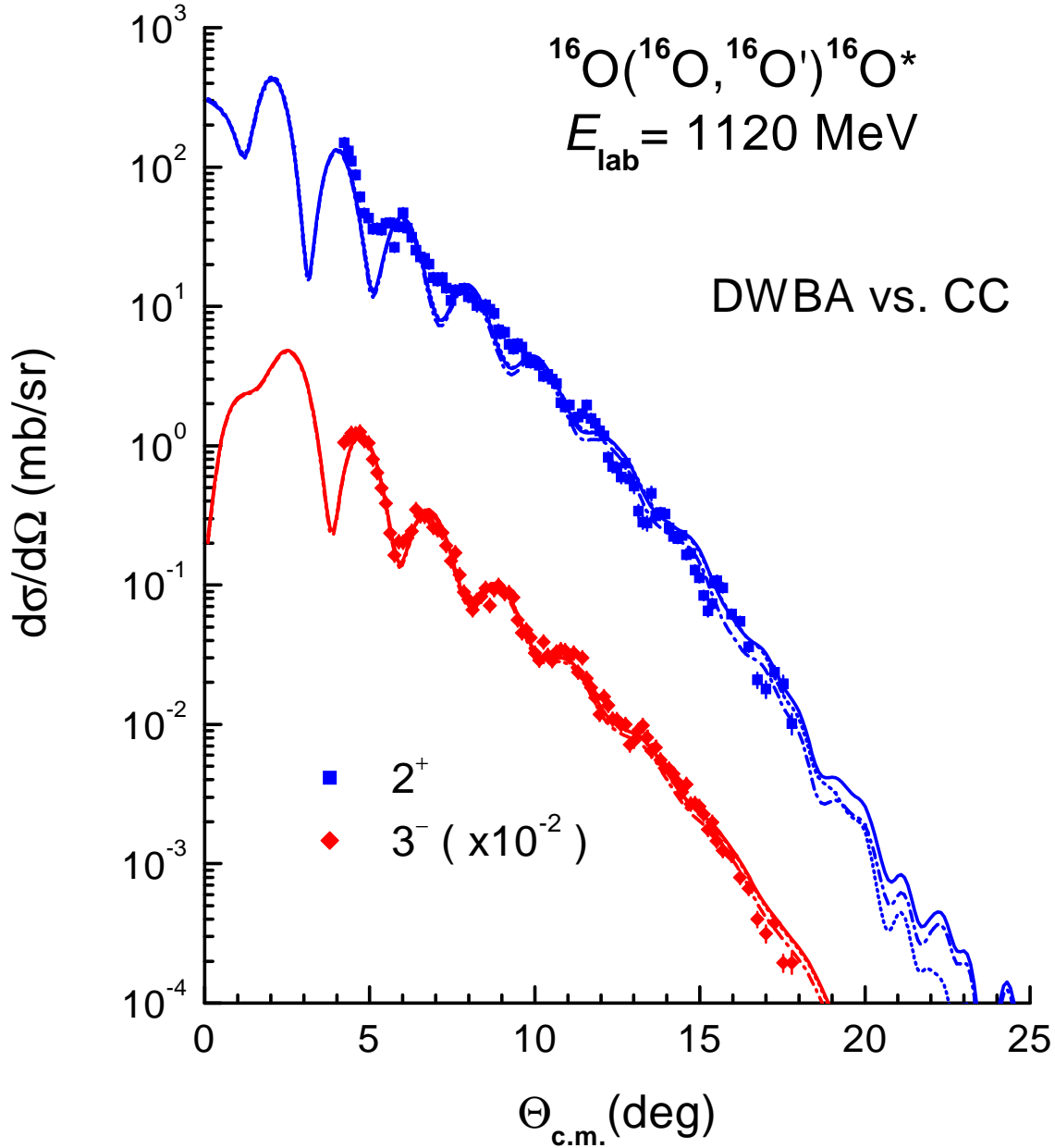


Fig. 4. The cross sections of the inelastic $^{16}\text{O}(^{16}\text{O}, ^{16}\text{O}')^{16}\text{O}^*$ scattering at $E_{\text{lab}} = 1120 \text{ MeV}$ in comparison with the data. The solid curves were calculated in the DWBA (see explanation for solid curves in Fig. 3); dash-dotted curves are given by the CC calculation using the same FF and OP parameters as those used for solid curves, but taking into account the 3-channel coupling $2^+ \leftrightarrow 0^+ \leftrightarrow 3^-$; dotted curves were obtained in the same CC scheme, but with the WS parameters of the imaginary OP slightly re-adjusted to best fit the data.

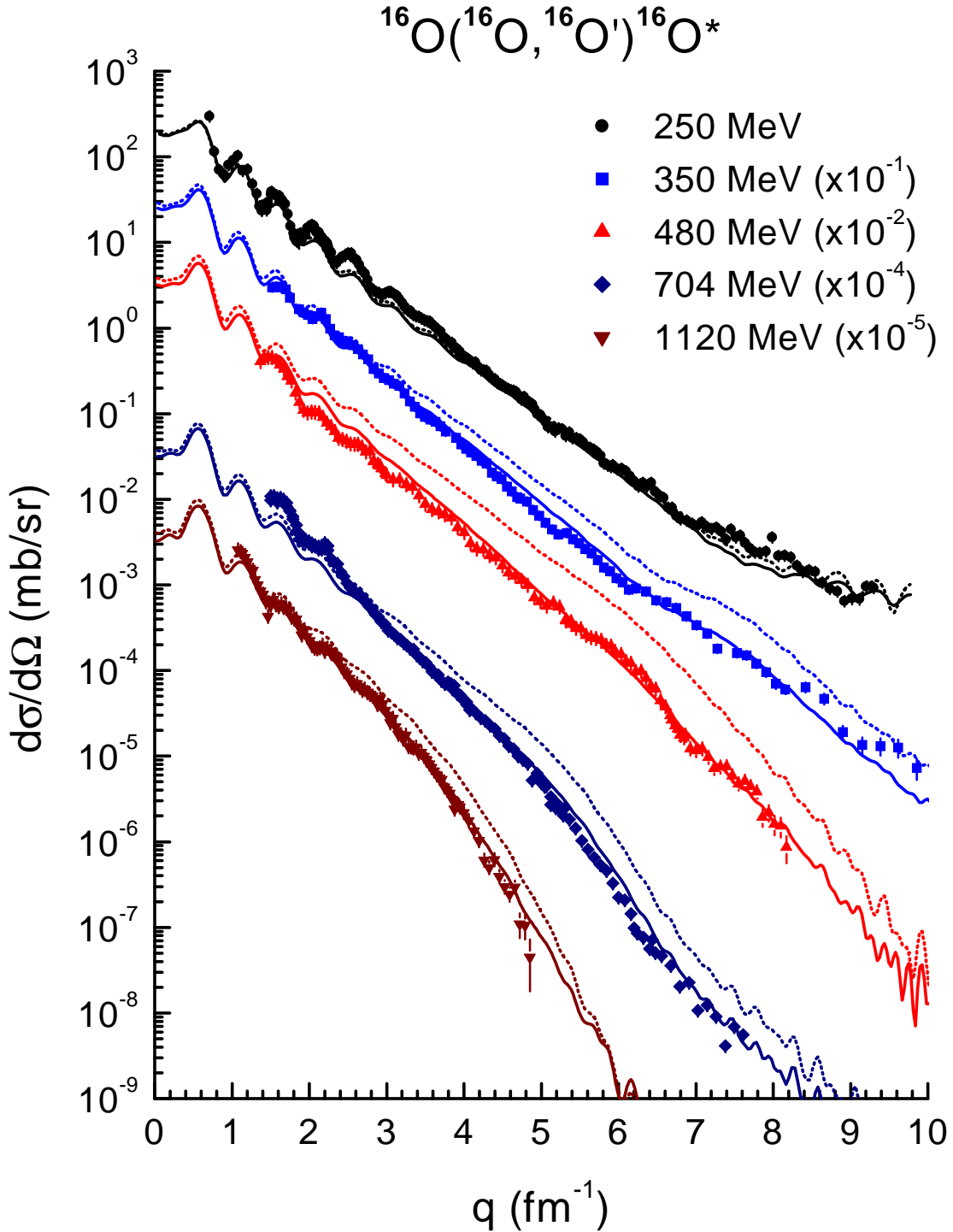


Fig. 5. The DWBA description of the measured total ($2^+ + 3^-$) inelastic $^{16}\text{O}(^{16}\text{O}, ^{16}\text{O}')^{16}\text{O}^*$ scattering cross sections at $E_{\text{lab}} = 250 - 1120$ MeV given by the original ($N_V^{(2,3)} = 1$) real folded FF. The dotted curves were obtained with the same complex OP for the entrance and exit channels, and the solid curves were obtained with a more absorptive OP in the exit channels (see Table 1). The cross sections are plotted versus the momentum transfer $q = 2k \sin(\Theta_{\text{c.m.}}/2)$, where k is the wave number of the projectile.

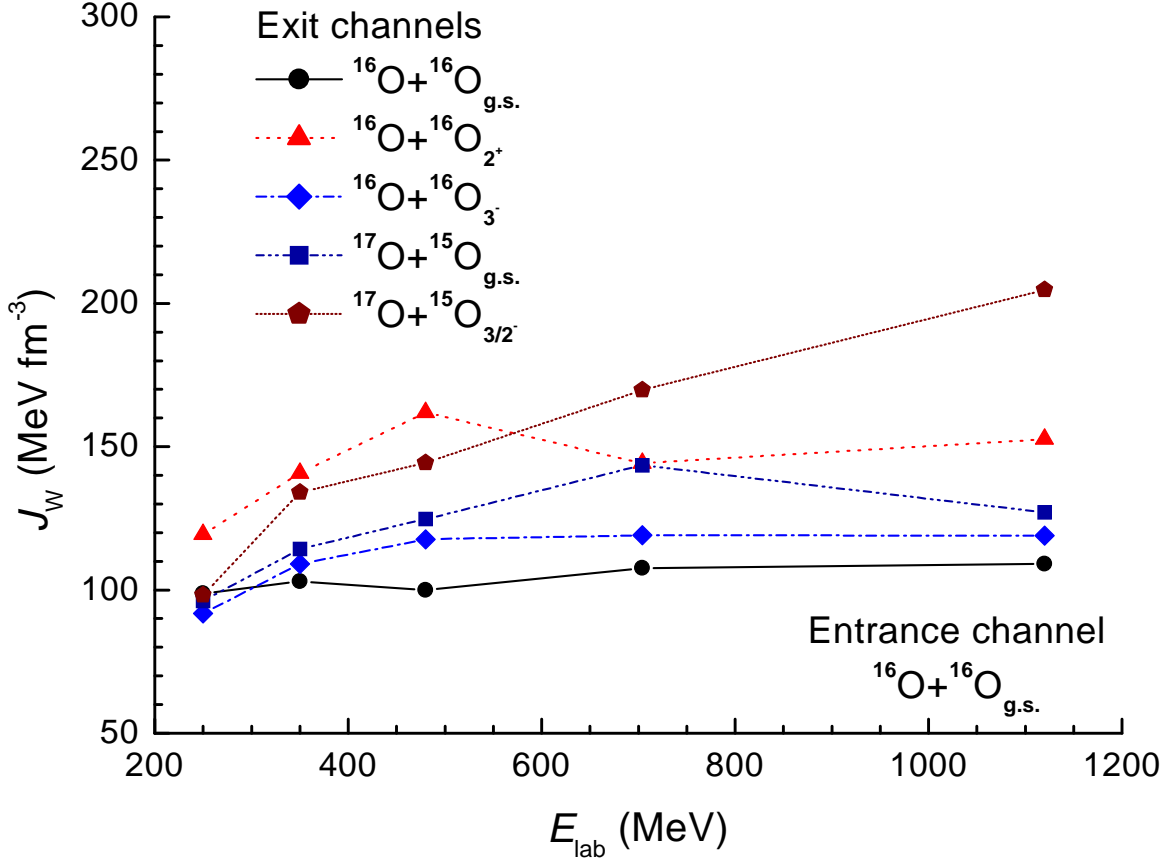


Fig. 6. Energy dependence of the volume integral per interacting nucleon pair J_W of the WS imaginary OP used for the elastic $^{16}\text{O}+^{16}\text{O}$ channel, $^{16}\text{O}+^{16}\text{O}_{2^+}$ and $^{16}\text{O}+^{16}\text{O}_{3^-}$ exit channels of the inelastic $^{16}\text{O}(^{16}\text{O},^{16}\text{O}')^{16}\text{O}^*$ scattering, and the exit channels of the one-neutron $\phi 17\text{o}15$ transfer [5] to the ground state $^{15}\text{O}_{\text{g.s.}}$ and the excited state $^{15}\text{O}_{3/2^-}$. The lines are only to guide the eye.

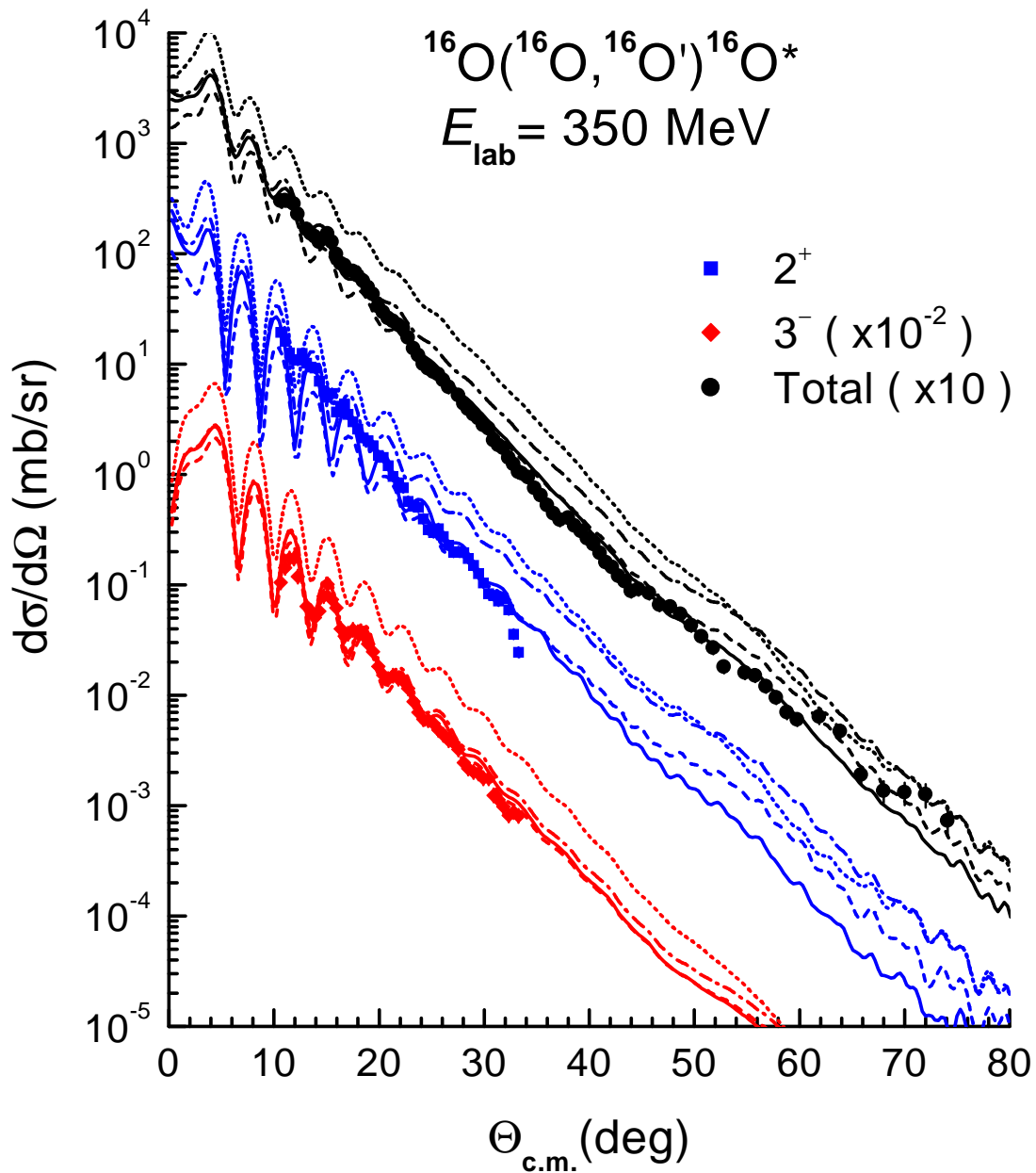


Fig. 7. The same as Fig. 3 but for $E_{\text{lab}} = 350 \text{ MeV}$.

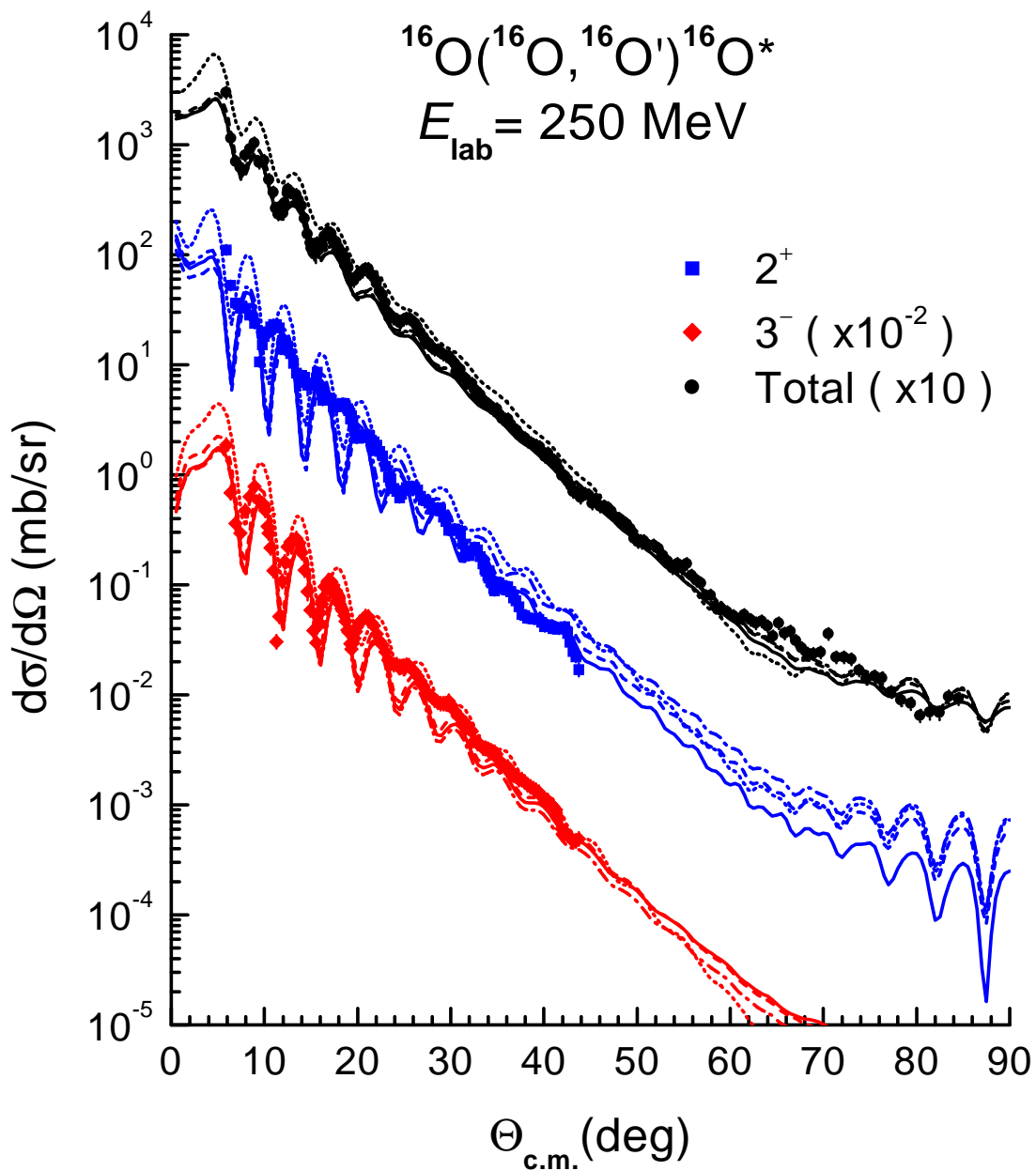


Fig. 8. The same as Fig. 3 but for $E_{\text{lab}} = 250 \text{ MeV}$.

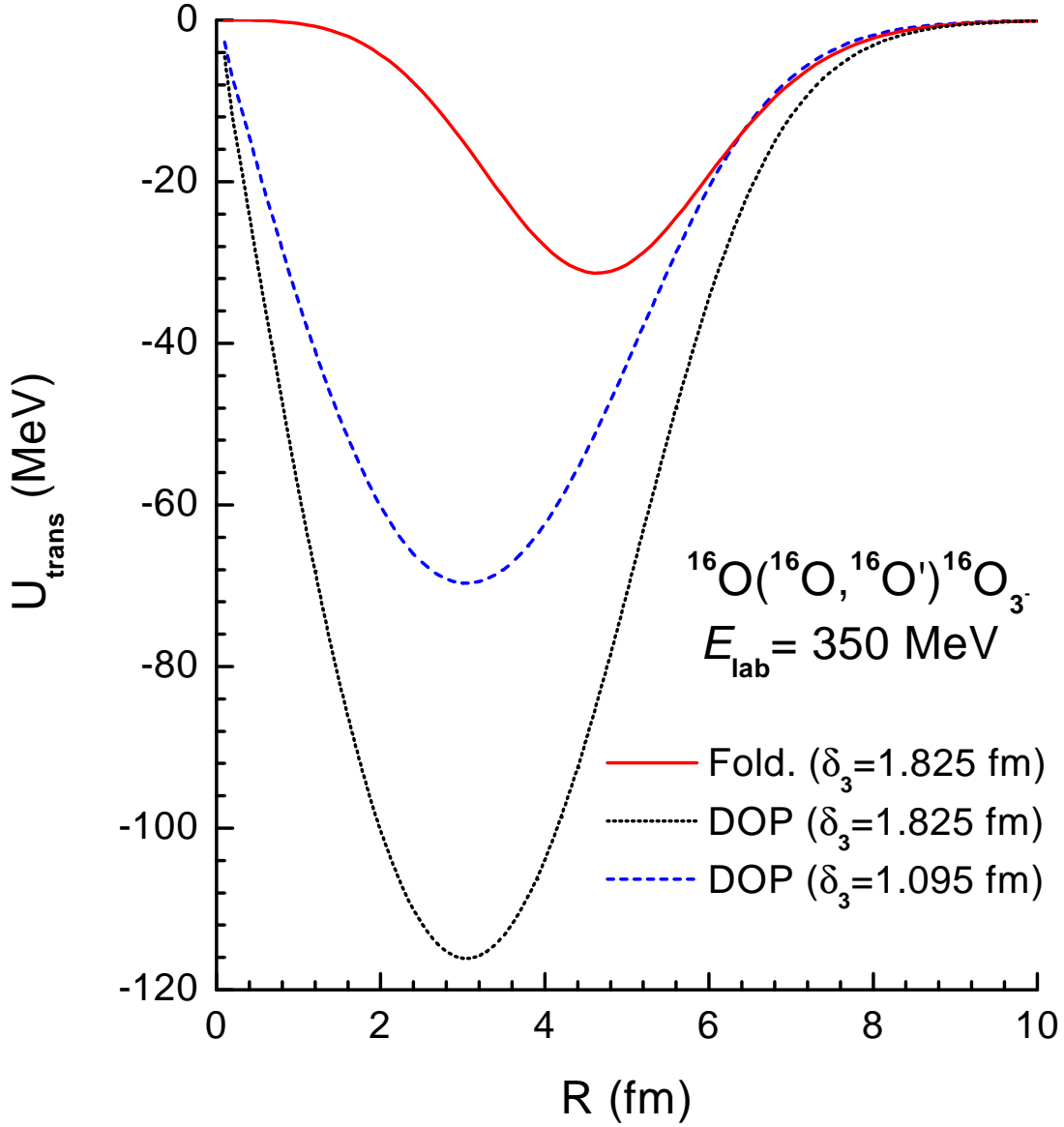


Fig. 9. The form factors for the transition $0^+ \rightarrow 3^-$ in the inelastic $^{16}\text{O}+^{16}\text{O}$ scattering at 350 MeV. The folded $V_{\text{F}}^{(3)}$ form factor is the solid curve, the DOP curves represent the best-fit elastic folded potential deformed with the same deformation length δ_3 as that used to generate $V_{\text{F}}^{(3)}$ (dotted curve) or with δ_3 adjusted to the best DWBA fit to the inelastic scattering data (dashed curve).

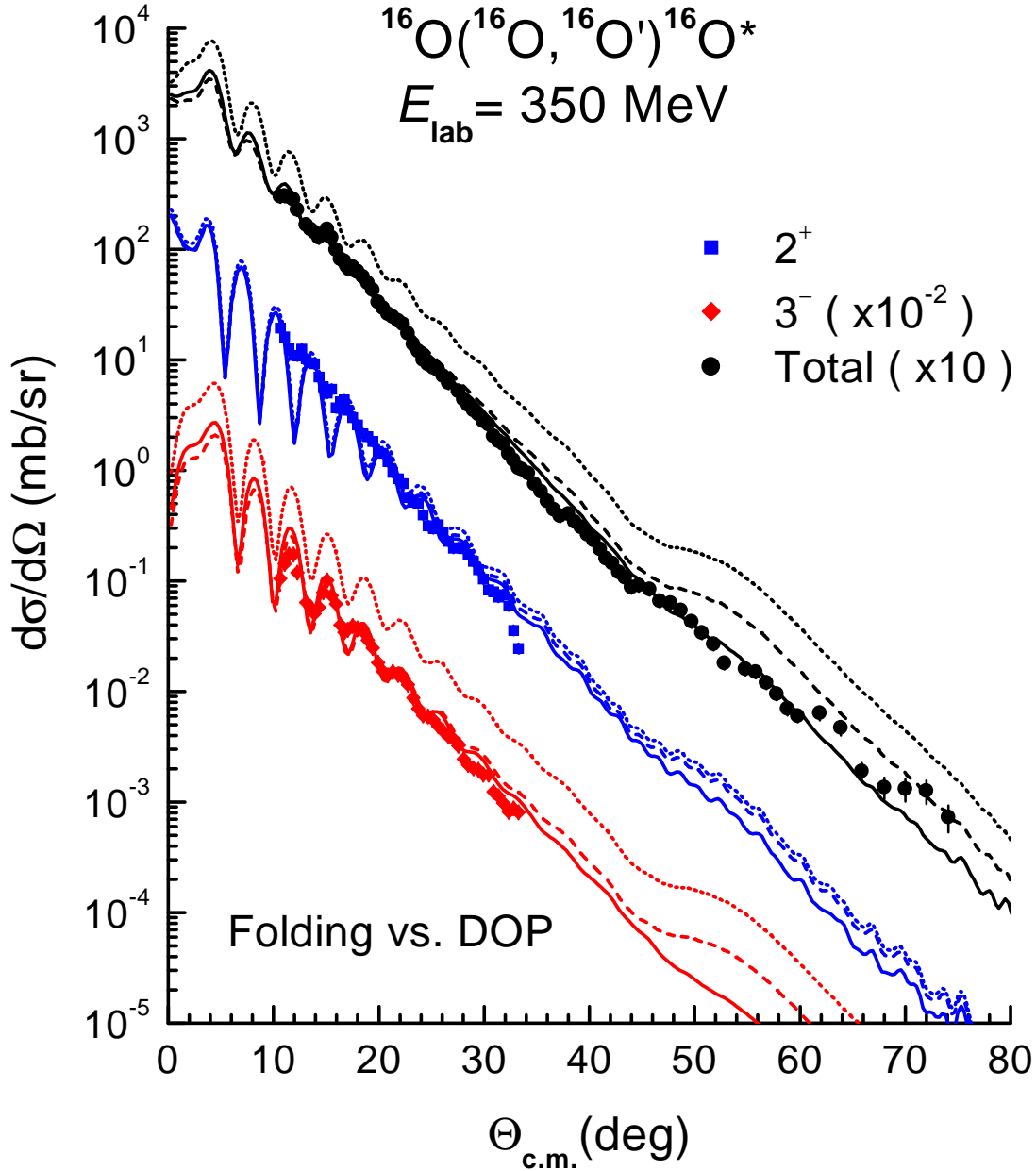


Fig. 10. The calculated DWBA cross sections for the inelastic $^{16}\text{O}(^{16}\text{O}, ^{16}\text{O}')^{16}\text{O}^*$ scattering at $E_{\text{lab}} = 350 \text{ MeV}$ in comparison with the measured 2^+ and 3^- inelastic cross sections and their sum. The solid curves were obtained with the same folded form factors $V_{\text{F}}^{(2,3)}$ as those discussed in Fig. 7, dotted curves were obtained with the DOP form factors built upon the same deformation lengths $\delta_{2,3}$ as those used to generate $V_{\text{F}}^{(2,3)}$, and dashed curves are the DOP results but with $\delta_{2,3}$ adjusted to the best DWBA fit to the data.